Evidence for complex multistability in photomagnetic cobalt hexacyanoferrates from combined magnetic and synchrotron x-ray diffraction measurements

Isabelle Maurin,[1,*] Dmitry Chernyshov,[2] François Varret,[3] Anne Bleuzen,[4] Hiroko Tokoro,[5,6] Kazuhito Hashimoto,[5] and Shin-ichi Ohkoshi[5,6]

[1]*Laboratoire de Physique de la Matière Condensée, Ecole Polytechnique, CNRS, 91128 Palaiseau Cedex, France*

[2]*Swiss-Norwegian Beam-Lines, European Synchrotron Radiation Facility, BP 220, 38048 Grenoble Cedex, France*

[3]*Groupe d'Etude de la Matière Condensée, Université de Versailles, CNRS, 45, Avenue des Etats-Unis, 78035 Versailles Cedex, France*

[4]*Laboratoire de Chimie Inorganique, Université d'Orsay, CNRS, Bât 420, 91405 Orsay, France*

[5]*Department of Applied Chemistry, School of Engineering, The University of Tokyo, 7-3-1 Hongo, Bunkyo-ku, Tokyo 113-8656, Japan*

[6]*Department of Chemistry, School of Science, The University of Tokyo, 7-3-1 Hongo, Bunkyo-ku, Tokyo 113-0033, Japan*

(Received 28 October 2008; revised manuscript received 7 January 2009; published 26 February 2009)

Cobalt hexacyanoferrates, which exhibit thermally induced and photo-induced spin transitions, have been extensively studied as model materials for molecular-based photomagnetic solids. Synchrotron x-ray diffraction (XRD) experiments combined with magnetic measurements were used here to get some new insights in their diagram of phase transformation. For a $Na_{0.32}Co[Fe(CN)_6]_{0.74}\cdot 3.4H_2O$ sample composition, the high-temperature (HT) phase could be efficiently trapped by rapid cooling, thus allowing a comparison with the photo-induced phase directly formed at low temperature by light irradiation. In terms of magnetic behavior, the two metastable phases strongly differ with lower critical temperature and magnetization values but higher decay temperature for the HT quenched phase. As only a slight change in the lattice constant with no symmetry breaking is reported from XRD, the differences between the two phases are discussed on the basis of local and disordered tilting of the $[Fe(CN)_6]$ polyhedral units.

DOI: 10.1103/PhysRevB.79.064420 PACS number(s): 75.50.Xx, 75.30.Wx, 64.60.My, 64.70.K−

I. INTRODUCTION

The optical control of materials properties in transition-metal oxides[1] and molecular solids[2,3] has drawn considerable attention during the past years. Photoexcitation can trigger electronic excitations, which then collectively propagate through the crystal leading to a new transient[4] or long-lived[5] phase. This phenomenon is commonly referred to as photo-induced phase transition (PIPT). Among such photoactive solids, Prussian blue analogs have attracted a great interest since they exhibit various photo-induced magnetization effects (light-induced ferrimagnetism[3] or demagnetization[6] and photocontrolled magnetic pole inversion[7]) with potential applications in memory devices and magneto-optical switching.[8] For instance, the extensively studied cobalt hexacyanoferrates, $A_xCo[Fe(CN)_6]_y\cdot zH_2O$ (A: alkali metal) display a charge-transfer-induced spin transition (CTIST), $Co^{III}(LS)(t_{2g}^6, S=0)$-$Fe^{II}(LS)(t_{2g}^6, S=0) \rightarrow Co^{II}(HS)(t_{2g}^5e_g^2, S=3/2)$-$Fe^{III}(LS)(t_{2g}^5, S=1/2)$, (where HS and LS denote high spin and low spin, respectively), on heating or, at low temperature, under light irradiation.[3] The photo-induced state orders ferrimagnetically below ~20 K, the magnetic interactions being mediated by the CN moieties, which connect the transition-metal ions in a three-dimensional (3D) network. For some of these compounds, the spontaneous (or thermal) CTIST is discontinuous[9] and the relaxation of the light-induced metastable state has a self-accelerated character,[10] these two characteristics being reminiscent of the spin-crossover phenomenon in molecular solids. Correspondingly, the equilibrium and photo-induced properties of these systems have been described in the frame of the two-level Ising-like model[11,12] developed for photoswitcheable spin-crossover complexes.[13] This latter approach considers the fraction of $Co^{II}(HS)$-$Fe^{III}(LS)$ pairs as the only order parameter and therefore does not distinguish between the thermally induced phase and the photoexcited (PX) phase, although the formation of these two phases proceeds through different mechanisms.

Recently, Huai and Nasu[14] suggested that photoexcitation at low temperatures, where the effect of thermal fluctuations is minimal, may give rise to new metastable phases normally hidden at thermal equilibrium, a concept called "hidden multistability." Experimental reports that corroborate this conjecture are restricted to only one case so far, based on Raman spectroscopy measurements on a spin-crossover complex $[Fe(2\text{-pic})_3]Cl_2EtOH$.[15] However, these results have not been confirmed by diffraction[16] or x-ray absorption fine structure (XAFS) (Ref. 17) data. Cobalt hexacyanoferrates could serve as model systems to study such hidden multistability. Indeed, the $Co^{II}(HS)$-$Fe^{III}(LS)$ metastable state can be generated at low temperatures, either by thermal quenching of the high-temperature (HT) state or by light irradiation of the low-temperature (LT) ground state. However, the corresponding macroscopic phases have not been thoroughly characterized yet, and little information is available concerning the structural changes associated with the thermally induced and photo-induced phase transitions.

Early XAFS spectroscopy measurements reported that the major structural modifications occur in the vicinity of the cobalt ions, with a rather large Co-N bond lengthening (~0.18 Å) that accompanies the $Co^{III}(LS) \rightarrow Co^{II}(HS)$ spin transition.[18] This transition is mentioned as isostructural with only a change in the volume of the unit cell.[19,20] No

significant differences could be detected between the high-temperature state and the photoexcited state, at least from XAFS measurements carried out at the Co and Fe K edges.[21] On the other hand, synchrotron x-ray powder-diffraction experiments have suggested a decreased lattice parameter for the HT quenched phase with respect to the photoexcited phase for a $Na_{0.42}Co[Fe(CN)_6]_{0.78}\cdot 4.6H_2O$ sample.[19] This observation was interpreted by a partial relaxation of the quenched phase toward the LT phase (~40%), leading to a lattice contraction related to elastic stresses induced by the relaxed matrix. It is worth mentioning that opposite results (increased lattice constant for the HT quenched phase as compared to the photoexcited phase) were reported for the $Rb_{0.73}Mn[Fe(CN)_6]_{0.91}\cdot 1.4H_2O$ system.[22]

More recently, XAFS measurements on a cesium-based cobalt hexacyanoferrate reported a displacement of the alkali-metal ions within the tetrahedral sites of the fcc structure at the thermal spin transition.[23] This displacement is accompanied by a change in the Co-NC-Fe arrangement, from bent to linear on cooling, in the close neighborhood of the alkali-metal ion. Such a tilting of the $[CoN_6]$ and $[Fe(CN)_6]$ polyhedral units would be of primary importance since the magnetic interactions proceed via superexchange coupling through the cyanide bridges. However, these XAFS measurements carried out at the Cs L_3 edge have not been supplemented yet by an accurate diffraction study in order to check whether these local distortions are correlated.

II. EXPERIMENT

The synthesis procedure and characterization of the $Na_{0.32}Co[Fe(CN)_6]_{0.74}\cdot 3.4H_2O$ sample studied in the present paper are detailed in Ref. 11. This composition was chosen so as to minimize the temperature interval between the cooling branch of the thermal hysteresis loop and the temperature decay of the quenched phase. This allows an efficient trapping of the high-temperature phase for both rapid[24] and flash[11] cooling procedures. According to Mössbauer and infrared spectroscopy measurements, the room-temperature phase mainly consists of Co^{II}-Fe^{III}(LS) pairs with a small admixture of Co^{II}-Fe^{II}(LS).

The raw sample was first submitted to several cooling$\leftrightarrow$warming sequences. Because of the large volume change ($\Delta V/V \sim 9\%$) associated to the spin transition, these cycles may induce some cracks, which would in turn affect the hysteretic properties of the sample. The dc magnetization was measured with a superconducting quantum interference device (SQUID) magnetometer (Quantum Design MPMS-5) equipped with an optical fiber connected to a laser diode system ($\lambda = 690$ nm, 30 mW output power). For the photoexcitation experiments, a thin layer of powder sample was deposited onto a transparent double-stick tape and placed directly at the end of the fiber. To compensate for the asymmetric SQUID response signal due to the magnetic contribution of the fiber guide, background scans were systematically recorded for the various measuring conditions and subtracted prior to fitting with the appropriate second-order gradiometer function. Wavelength suitable for photoexcitation was deduced from previous studies.[3,25,26] $A_xCo^{III}[Fe^{II}(CN)_6]_y\cdot zH_2O$ compounds show a very broad metal-to-metal charge-transfer (MMCT) band, centered around 550 nm, which is weakly dependent on the nature and on the concentration of the alkali-metal ion. Following the work of Romstedt *et al.*,[27] the irradiation wavelength was tuned to the tail of the MMCT transition, where the optical density is reduced, to prevent large intensity gradients within the crystallites and thus limit their risk of cracking.

For structural studies, a powder sample was sealed under helium gas in a 0.1 mm-diameter glass capillary and synchrotron x-ray diffraction (XRD) data were collected at the Swiss-Norwegian Beam Lines (station BM1A) at the European Synchrotron Radiation Facility in France. A monochromatic beam of wavelength $\lambda = 0.8198(1)$ Å was focused onto the sample by sagital bending of the second crystal of a double-crystal Si(111) monochromator. Images of the Debye-Scherrer rings were recorded on a 345-mm-diameter Mar Research image plate system. Capillaries were spun around their axis by 60° during data acquisition, and images were collected in the dose mode (~60 s) with a sample-to-detector distance of 280 mm. Homogeneous intensity distribution in the Debye rings indicated well-randomized crystallites. One-dimensional diffraction patterns were then extracted by integration using the FIT-2D software.[28] Si powder NIST standard was used to calibrate the sample-to-detector distance, beam center, and tilt angle of the image plate detector. Temperature-dependent measurements were performed using an Oxford Cryostream nitrogen blower. Sweep rates were limited to 0.5 K min^{-1} in the region of the spontaneous transition, but increased to 1 K min^{-1} elsewhere. The photoexcitation experiments were carried out with the same light source as the one used for the magnetic measurements.

III. RESULTS

A. Magnetic and switching properties

Dc-magnetization measurements were first performed as a function of temperature on a rather large amount of sample (~3 mg). Between 190 and 260 K, a steep change in magnetic susceptibility occurs with a broad kinetics-dependent hysteresis, indicative of the Co^{III}(LS, $S=0$)-Fe^{II}(LS, $S=0$)$\leftrightarrow$$Co^{II}$(HS, $S=3/2$)-Fe^{III}(LS, $S=1/2$) spontaneous charge transfer (see Fig. 1). The descending branch of the thermal loop was found to be particularly sensitive to the cooling rate down to 0.25 K min^{-1}. When the sweep rate is increased, this branch is first shifted toward low temperature and then the transition becomes incomplete with an increasing fraction of Co^{II}-Fe^{III} pairs trapped at low temperature. In the following, the low- and room-temperature phases will be referred to as LT phase and HT phase, respectively.

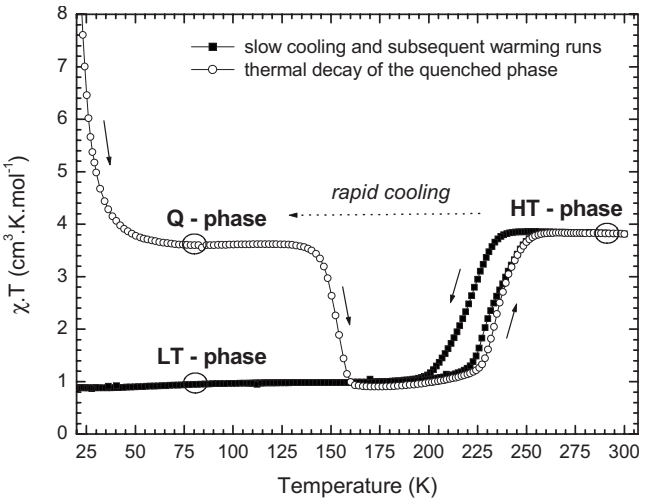

FIG. 1. Temperature-dependent magnetic susceptibility measurements in the cooling and subsequent warming runs (close symbols), applied magnetic field: 4000 Oe, sweep rate: 0.75 K min^{-1} except in the range 180–270 K where it was reduced to 0.45 K min^{-1}. Comparison is shown with the data recorded during the thermal decay of the HT quenched phase (open symbols).

1. HT quenched phase

The magnetic-susceptibility data recorded after cooling rapidly the sample down to 30 K are also reported in Fig. 1. As the temperature is further lowered, χT shows a steep increase indicating a magnetic ordering of the HT quenched phase. The curvature of the $1/\chi$ versus T plot agrees with ferrimagnetic order with predominant antiferromagnetic interactions between Co^{II} and Fe^{III} nearest neighbors.[29] The χT value at 90 K, 3.60 cm^3 K mol^{-1} is slightly lower than that measured at room temperature, 3.83 cm^3 K mol^{-1}. However, χT displays a slight increase on increasing temperature, also observed for the LT phase (major contribution of Co^{II} ions because of a Co/Fe ratio larger than one in the sample under study). It is therefore difficult to estimate a fraction of Co^{III}-Fe^{II} relaxed pairs if any.[30] Nevertheless, owing to the reproducibility of the quenching experiments (see Ref. 31), a comparison with the Mössbauer measurements[11] for which we used flash cooling rather than rapid cooling is relevant, and a mere Co^{II}-Fe^{III} formal electronic configuration—identical to that of the HT state—should be inferred for the quenched (Q) state.

For this metastable phase, magnetization loops are consistent with an onset of magnetic order below 16.4 K, the temperature at which the remanent (RM) magnetization is no longer detectable within the magnetometer sensitivity [Fig. 2(a)]. The $M(H)$ curve at 5 K yields a maximum value under 5 T, M_{max} of $2.3\mu_B$ per $Na_{0.32}Co[Fe(CN)_6]_{0.74}\cdot 3.4H_2O$ unit [see Fig. 2(b)]. This value strongly deviates from the saturation value, $\sim 3.2\mu_B$.

On warming, the decay of the HT quenched phase is observed at 154 K (Fig. 1). This temperature was arbitrarily defined as the inflection point of the χT vs T curve and will be denoted T_d in the following. For $T > T_d$, deviations with respect to the measurements performed in quasi-equilibrium

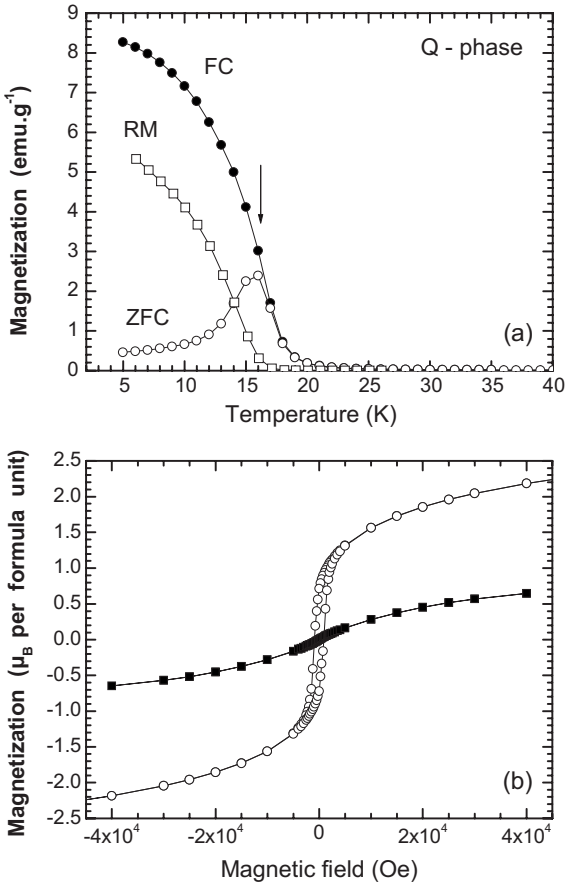

FIG. 2. (a) Zero-field-cooled (ZFC) and field-cooled (FC) magnetization measurements under 50 Oe carried out on the $Na_{0.32}Co[Fe(CN)_6]_{0.74}\cdot 3.4H_2O$ sample after rapid cooling to 30 K. The temperature decay of the remanent (RM) magnetization is also presented. The arrow marks the inflection point of the $M_{FC}(T)$ curve, 16.2 K. (b) Magnetization M versus H curves measured at 5 K for the HT quenched phase (open symbols) and for the slowly cooled LT phase (close symbols).

conditions are still observed, roughly up to 240 K, with magnetic susceptibility values lower than those reported for the LT phase.

2. Photoexcited phase

These data obtained on a rather large sample amount were used to calibrate the subsequent measurements, which were performed on a very thin-layer sample because light attenuation is particularly severe in these materials. The sample was slowly cooled down prior to photoexcitation, at 0.45 K min^{-1} to avoid quenching effects. Its mass (~ 30 μg) was then estimated by scaling the M-H curve measured at 5 K with that of the bulk sample. Irradiation was carried out at 10 K with $\lambda = 690$ nm and 50 mW cm^{-2} excitation power (see the inset of Fig. 3). Magnetization increased significantly during illumination, in agreement with an optically induced electron transfer, $Fe^{II}(LS, S=0) + Co^{III}(LS, S=0) \rightarrow Fe^{III}(LS, S=1/2) + Co^{II}(HS, S=3/2)$, accompanied by a magnetic ordering of the Co and Fe

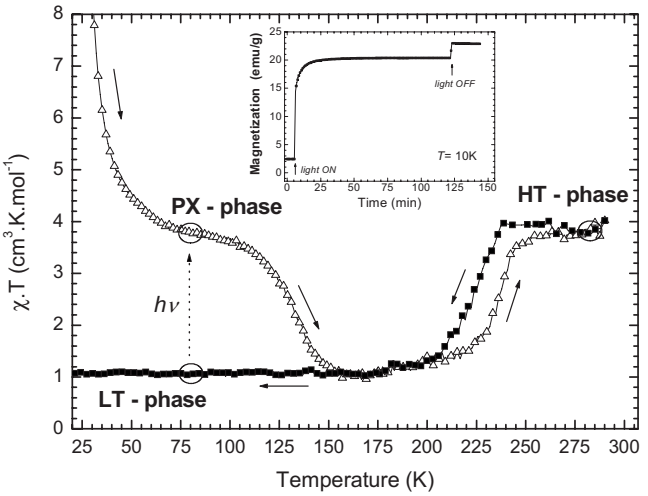

FIG. 3. Thermal decay of the photoexcited metastable phase (open triangles) and subsequent magnetic measurements in the cooling mode (close squares). The poorer quality of the data in the high-temperature range is due to the difficulty in measuring very small magnetic moments and sensitivity to a proper subtraction of the sample holder contribution. In inset: time-dependent magnetization change at 10 K under permanent irradiation, $H=4000$ Oe. The increased sample temperature during photoexcitation is responsible for the abrupt change in magnetization once the irradiation is stopped.

sublattices. Because of the rather small sample thickness, a steady state could be reached within 50 min and this metastable state was found to persist for several days at low temperature. The following measurements on the PX phase were carried out after a preliminary annealing at 40 K in the paramagnetic regime.[32]

The χT value at 90 K, 3.72 cm^3 K mol^{-1}, is comparable to that measured at room temperature and to the one recorded at 90 K after quenching, indicating a similar level

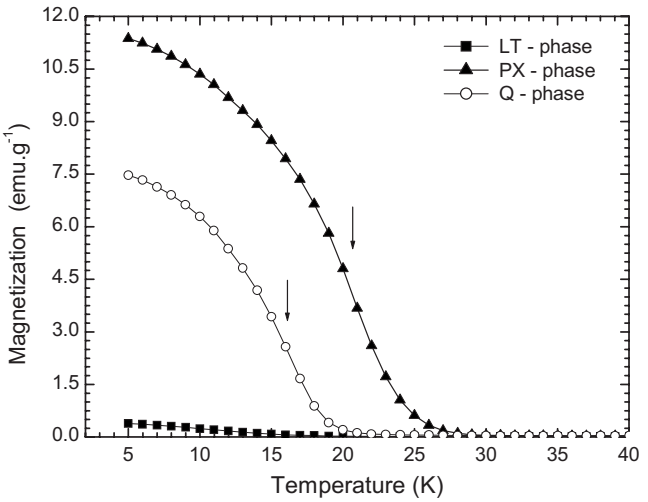

FIG. 4. Field-cooled magnetization, measured under ~50 Oe, for the HT quenched (Q) phase and the photoexcited (PX) phase. Comparison is shown with the LT phase obtained after slow cooling. The inflection points are marked by arrows.

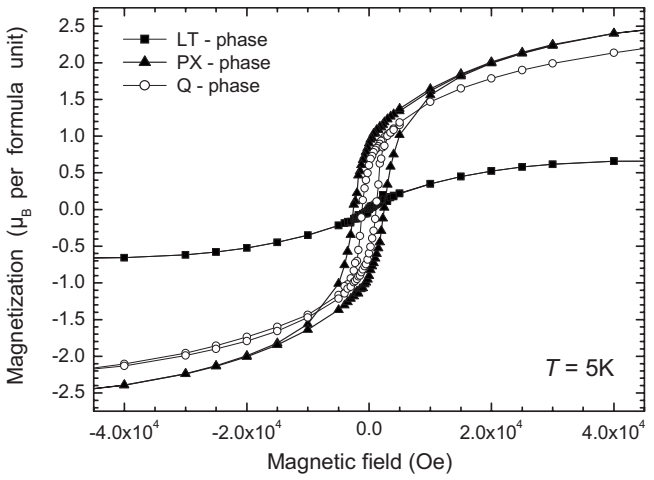

FIG. 5. Magnetization loops M-H measured at 5 K for the HT quenched phase, the photoexcited phase and the slowly cooled LT phase.

of Co^{II}-Fe^{III} pairs. Nearly all Co^{III}-Fe^{II} diamagnetic pairs have thus been converted during the irradiation process. Below 30 K, the large increase in χT marks an onset of ferrimagnetic order similar to that observed for the HT quenched phase. Field-cooled magnetization measurements with $H \sim 50$ Oe are displayed in Fig. 4 together with those recorded before illumination or after rapid cooling to 20 K. Compared to the Q phase, the photoexcited phase orders at higher temperature and display larger magnetization values (Figs. 4 and 5). In addition, the PX phase decays back to the quasi-equilibrium phase at lower temperature. This decay is also very gradual and smears over roughly 55 K, instead of 30 K for the Q phase.

Magnetic data characteristic of the LT ground state, the HT quenched state, and the photoinduced state are summarized in Table I. The reproducibility of the photoexcitation experiments was found to be very similar to that reported for the quenched sample (see Ref. 31). These uncertainties are thus far smaller than the differences between the quenched and photoexcited phases. Those macroscopic phases were then further characterized in terms of corresponding structural phases by means of synchrotron x-ray powder diffraction.

TABLE I. Selected magnetic data for the quasi-equilibrium LT phase and for the quenched and photoexcited metastable phases: χT value at 90 K; mean critical temperature, $\langle T_c \rangle$ as derived from Eq. (1) detailed in the discussion part; magnetization value at 5 K under 5 T, M_{max}; field-cooled magnetization value at 5 K under ~50 Oe, M_{FC}; decay temperature of the metastable phase, T_d.

	χT at 90 K (cm^3 K mol^{-1})	$\langle T_c \rangle$ (K)	M_{max} (emu g^{-1})	M_{FC} (emu g^{-1})	T_d (K)
LT phase	0.96		13	0.4	
Q phase	3.60	16.7	45	7.5	154
PX phase	3.72	21.2	49	11.4	132

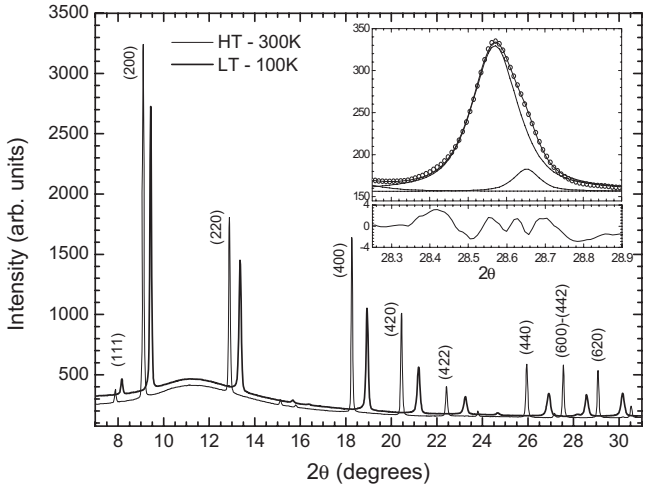

FIG. 6. Synchrotron x-ray diffraction profiles at 300 K and after slow cooling down to 100 K for $Na_{0.32}Co[Fe(CN)_6]_{0.74}\cdot 3.4H_2O$ ($\lambda=0.8198$ Å). In inset, enlarged view of the (600)-(442) line, collected at 100 K and modeled using two pseudo-Voigt functions. Top panel: experimental (open symbols) and calculated (solid line) profiles. Bottom panel: residue as an indication of the fit goodness.

B. Synchrotron x-ray diffraction

1. High-temperature phase

The diffraction profile of the $Na_{0.32}Co[Fe(CN)_6]_{0.74}\cdot 3.4H_2O$ sample was first collected at room temperature (see Fig. 6). Indexing gave a cubic unit cell of a parameter, 10.3216(3) Å, and the $Fm3m$ space group reminiscent of Prussian blue[33] is consistent with the systematic absences. The Bragg reflections were fitted with pseudo-Voigt (PV) functions, as implemented in the PEAKOC program,[34] and the lattice constant was determined by least-square refinement of the corresponding d spacings. Peaks are slightly broader than the instrumental resolution, e.g., 0.070° full width at half maximum (FWHM) for the (200) line and 0.078° for the (220) peak, to be compared to the instrumental contributions, 0.059° and 0.057°, at the corresponding Bragg angles. On cooling, the diffraction profiles showed the coexistence of HT-like and LT-like phases between 250 and 190 K, with large and small a parameter values, respectively. The detailed study of this two-phase region will be presented elsewhere.

2. Low-temperature phase

Compared to the data set collected at room temperature, the diffraction pattern of the LT phase reveals substantial changes in the position and in the width of the Bragg reflections (Fig. 6). All the diffraction peaks shift toward high 2θ angles, indicating a large volume contraction, $a=9.9625(6)$ Å at 100 K, as expected from the Co-N bond shortening that accompanies the $Co^{II}\rightarrow Co^{III}$ electron transfer. A significant peak broadening is apparent (also mentioned by Hanawa *et al.*[19] on a different sample), e.g., 0.083° and 0.113° FWHM for the (200) and (220) reflections, respectively. Nevertheless, the peak width that was measured at room temperature was fully recovered after warming back the sample to 300 K. A closer inspection of the low-temperature diffraction profile shows up a well-defined shoulder in the high-angle side of the (600) and (620) cubic reflections (see the inset of Fig. 6), which would actually account for phase separation or reduction in the crystal symmetry. These splittings were better resolved on data recently recorded at the High-Resolution Powder Diffraction Beamline (station ID31), ESRF. According to preliminary indexing attempts, the split lines could suggest a rhombohedral or an orthorhombic distortion of the double-perovskite structure. It is noteworthy that if phase separation was assumed, the majority phase would be considered as cubic whereas the minority phase should adopt a lower symmetry. Although the question of symmetry lowering in a single-phase materials or of macroscopic phase separation (due to chemical heterogeneities[35] or to a multivalley free-energy landscape) remains open, the thermodynamical state reached after slow cooling will be hereafter referred to as a single cubic phase for simplicity.

3. Photoexcited state

The PX phase was then prepared at 100 K by red light irradiation ($\lambda=690$ nm, ~ 0.1 W cm^{-2}, 2 h). The shift in 2θ of the (600) line is consistent with a ~ 10 K laser heating effect. A small amount of residual LT phase remained after the illumination was stopped [Fig. 7(a)], presumably because of bulk absorption effects that limits the penetration of the excitation light. After one-hour irradiation, the diffraction features of the light-driven phase and of this residual phase were found to vary very little. The fast data-acquisition capability of the image plate detector was then used to monitor the thermal decay of the photoexcited state after switching off the laser light.

The irradiation gave rise to a new phase with an increased lattice constant, $a=10.3015(3)$ Å at 100 K. The striking feature is the strong anisotropic peak broadening [inset of Fig. 7(a)], which shows up as a narrowing of the (h00) lines while the width of the other reflections remain virtually as broad as in the original LT phase. (200) and (220) lines could again serve as examples with 0.072° and 0.122° FWHM at $T=100$ K. This broadening could be the signature of some two-dimensional (2D) growth of photoexcited domains within the close-packed {111} planes. The formation of such plateletlike domains during photoexcitation has already been observed, from single-crystal x-ray diffraction experiments, in spin-crossover polymers presenting a strong 2D character.[36] This anisotropic peak broadening is partly released on heating before the electronic relaxation, $Co^{II}(HS)+Fe^{III}\rightarrow Co^{III}(LS)+Fe^{II}$, takes place.

It is important to mention that below 145 K all the diffraction lines assigned to the photo-induced phase can be well reproduced using single PV functions in clear contrast with what was reported for the LT phase. No splitting could be resolved and this result was confirmed by high-resolution XRD experiments performed on the ID31 beamline. The decay of the light-induced phase occurs between 145 and 170 K. In this temperature interval, the diffraction patterns show the coexistence of PX-like and LT-like phases. At 180 K, the

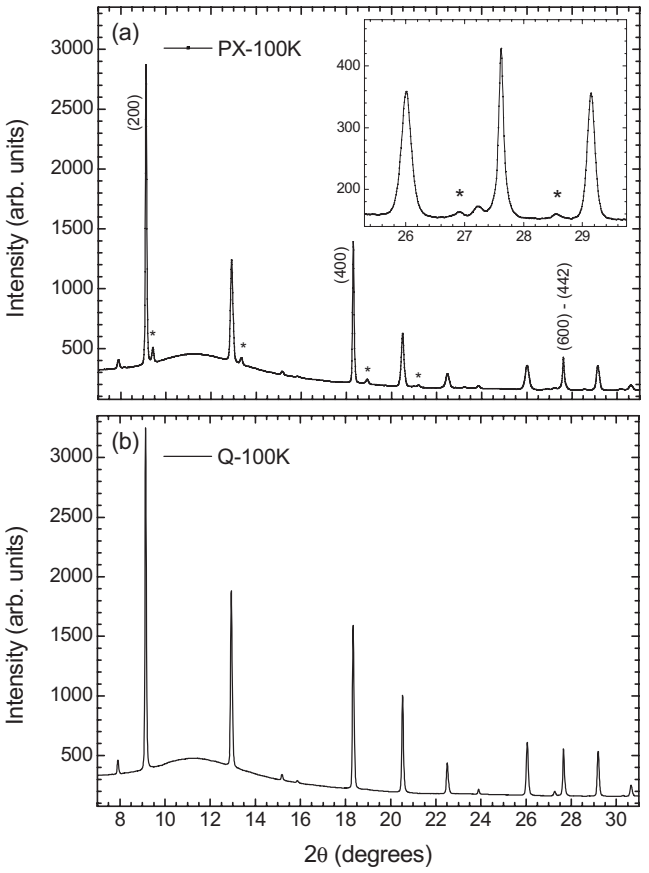

FIG. 7. Synchrotron x-ray diffraction patterns at 100 K: (a) photoexcited (PX) phase and (b) high-temperature quenched (Q) phase. On the top panel, asterisks mark the major peaks of the residual low-temperature phase.

profile of the relaxed phase is found to be identical to that of the LT phase measured during the cooling run (Fig. 8).

4. HT quenched phase

The sample was flash cooled down to 100 K [Fig. 7(b)] and the efficiency of the cooling protocol was confirmed by the absence of significant peak broadening (see Table II). As for the HT phase, all diffraction peaks could be very well fitted using single PV functions. The a-cubic parameter value

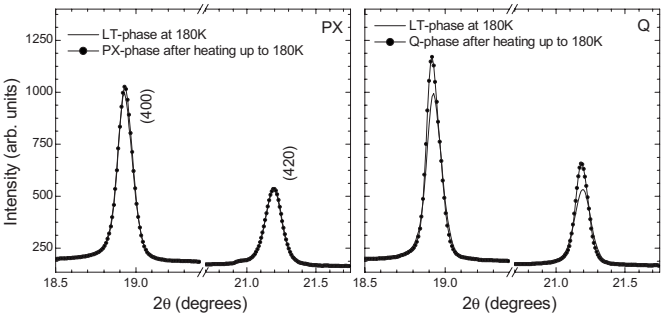

FIG. 8. Comparison between the diffraction profiles of the slowly cooled phase and of the PX (or Q) phase after relaxation at 180 K.

TABLE II. Selected structural data for the HT and LT phases and for the quenched and photoexcited metastable phases: lattice parameter, a; Full width at half maximum (FWHM) for the (200) and (220) diffraction lines.

	Lattice constant, a (Å)	FWHM (200) (deg)	FWHM (220) (deg)
HT phase	10.3216(3) at 300 K	0.0703(8)	0.078(1)
LT phase	9.9625(6) at 100 K	0.083(1)	0.113(2)
PX phase	10.3015(3) at 100 K	0.0721(9)	0.122(2)
Q phase	10.2862(3) at 100 K	0.0716(8)	0.079(1)

determined at 100 K is 10.2862(3) Å. When the temperature is raised, this metastable phase shows very little change in its lattice parameter value unlike the photoexcited phase (see Fig. 9). Its decay process is also quite different. The formation of the relaxed phase (with reduced lattice constant) is shifted to higher temperatures, above 155 K, in agreement with the magnetic measurements. The electronic relaxation

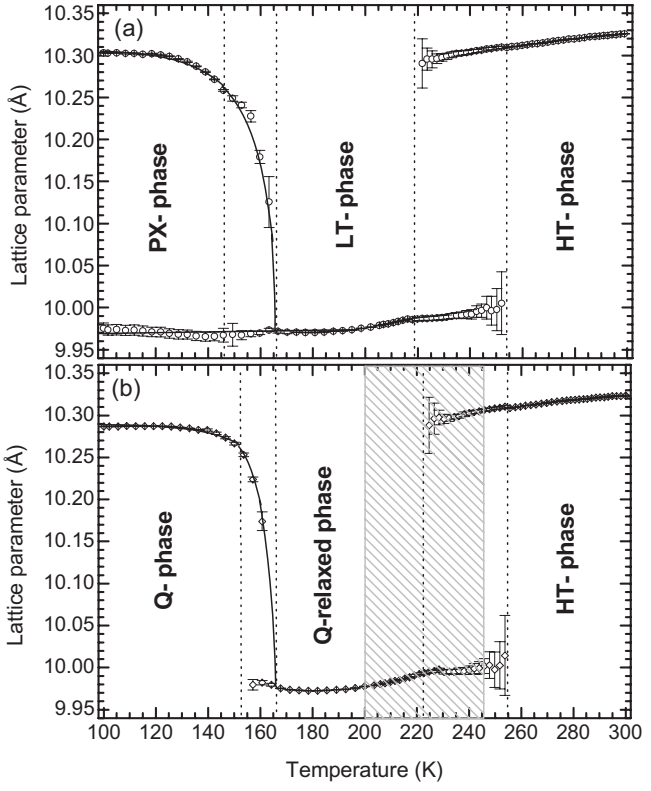

FIG. 9. Temperature dependence of the cubic lattice-parameter value, derived from the d_{220} spacing, measured on warming for the (a) photoexcited phase and the (b) HT quenched phase. This Bragg peak was chosen because it could be fairly well reproduced by a single PV function in all data sets. These data are not directly comparable to Figs. 1 and 3 because of a different sweeping rate in the 100–180 K range. Dotted lines mark the boundaries of clearly resolved two-phase regions. In these temperature intervals, the diffraction lines were modeled by split pseudo-Voigt functions to account for the strong lineshape asymmetry. The hatched zone defines the temperature range in which the Q-relaxed phase is converted into the LT phase.

leads to a phase which lattice constant is close to that of the LT phase but with sharper diffraction lines (Fig. 8). For this new phase which will be referred to as *Q -relaxed phase*, a well-defined splitting of the (400), (600), and (620) Bragg reflections is again apparent, but other peaks such as (422) and (440) remain well modeled using single PV functions contrary to what was observed for the LT phase.

Above 200 K, a broadening of the diffraction lines together with a decrease in their intensity marks the decay of this secondary phase into the LT phase. This transformation occurs on a rather large temperature interval, up to roughly 245 K (Fig. 9). At this temperature, the fraction of HT phase could be estimated as 86% from the relative intensity of the (220) line. This result is consistent with the magnetic-susceptibility data reported in Fig. 1, which shows that the back conversion of the *Q*-relaxed phase into the equilibrium phase is complete above 240 K. Higher resolution x-ray diffraction data, eventually collected on single crystals, would be necessary to uncover the underlying structural differences between the *Q*-relaxed and LT phases.

For the various phases, the lattice constant value and the width of some characteristic Bragg peaks are listed in Table II. To summarize the conclusions derived from the diffraction data, we have plotted in Fig. 9 the variation in the unit-cell constant on warming, after (a) photoexcitation and (b) thermal quenching.

These structural data corroborate the results of the previous magnetic study. All together they show clear differences not only in the diffraction patterns of the PX and *Q* phases, but also in their thermal evolution. The nucleation of the Co^{III}-Fe^{II} relaxed phase is initiated at higher temperature for the *Q* phase with respect to the PX phase, which correlates well with the enhanced decay temperature, T_d, derived from the magnetic data. In addition, the XRD measurements have shown that the *Q* phase displays a two-stepwise back conversion into the equilibrium phase, which proceeds through first a charge-transfer-based relaxation into the *Q*-relaxed phase ($150\ \mathrm{K} < T < 170\ \mathrm{K}$) and then a structural transformation into the LT ground state ($200\ \mathrm{K} < T < 245\ \mathrm{K}$), the latter being very gradual. On the contrary, the PX phase relaxes directly toward the LT phase.

IV. DISCUSSION

In the following, we will only reconsider the differences in the magnetic properties of the photoexcited and HT quenched phases on the basis of the x-ray diffraction data. For mere purpose of comparison, the magnetization curves, $M_{\mathrm{FC}}(T)$ reported in Fig. 4 were approximated by the expression

$$\frac{M_{\mathrm{FC}}(T)}{M_{\mathrm{FC}}(0)} = \int_T^{\infty} \frac{1}{\sqrt{2\pi}\Delta T_c} \exp\left(-\frac{(T_c - \langle T_c\rangle)^2}{2\Delta T_c^2}\right) \cdot \left(\frac{T - T_c}{T_c}\right)^{\beta} dT_c, \tag{1}$$

which convolutes a scaling law for 3D Ising-like systems with a Gaussian distribution of local critical temperatures, T_cs.[37] The dependence of T_c with the applied magnetic field was neglected for simplicity and the critical exponent β was taken as 0.33.[38] The experimental data were fairly well modeled using a mean critical temperature, $\langle T_c\rangle$, of 21.2 K (16.7 K) and a spread, ΔT_c, of 2.7 K (2.2 K) for the photoexcited (quenched) phase. The most intriguing feature is the 21% increase in critical temperature for the PX phase that cannot be accounted for by a change in spin density (2% at most, see Table I).

The relative smearing of the magnetic transition for the photo-induced phase correlates rather well with the large broadening of the thermal decay reported for this phase. The spread of these two transitions is an indication of a large-scale disorder in the PX phase, which is also consistent with the broadening of the Bragg reflections. This measure of the structural coherence should not be mixed with short-range or uncorrelated disorder that would affect the Bragg intensities rather than the width of the reflections. Nonetheless, the presence of large defect densities (dislocations, cracks, etc.) would lead at worst to the formation of small magnetic clusters with short relaxation time and low freezing temperature, inconsistent with the higher $\langle T_c\rangle$ value reported for the PX phase. The differences between the quenched and photoexcited phases should therefore account for a change in the crystal structure.

The two phases are very similar in terms of corresponding diffraction patterns, except for a slightly increased lattice constant for the light-induced phase. The increased $\langle T_c\rangle$ value reported for this phase seems in apparent contradiction with the observed lattice expansion, which is expected to weaken the magnetic interactions. It follows that there must be a structural deformation that differentiates the PX and *Q* phases. However, the isostructural relationship between the two phases implies a nonsymmetry-breaking character of the corresponding deformation.

We propose here that the two structures differ in terms of local tilts of the corner-sharing $[Fe(CN)_6]$ and $[CoN_6]$ octahedra. Uncorrelated tilts averaged over the crystal would decrease the unit-cell dimension, preserving the average $Fm3m$ symmetry. For α being a local tilt, this scenario implies $\langle\alpha\rangle = 0$ but $\langle\alpha^2\rangle \neq 0$, and $\langle\alpha^2\rangle_{\mathrm{PX}} < \langle\alpha^2\rangle_Q$. A large buckling of the Fe-CN-Co chains in the *Q* phase would efficiently reduce the magnetic exchange interactions and hence lead to a lower $\langle T_c\rangle$ value. It is worth mentioning that this model of local rotations of the $[Fe(CN)_6]$ units agrees with the bending of the Co-NC-Fe chains, which was detected in the HT phase at the vicinity of the alkali-metal ions by XAFS.[23] Such tilts of the polyhedral units, presumably dynamic in nature, were also recently invoked to explain the invarlike behavior[39] or negative thermal expansion[40] in several Prussian blue derivatives. Following Ref. 23, some or all these tilts would be suppressed in the LT phase, and one could assume that the photoexcited phase adopts even more linear arrangements; this would imply that $\langle\alpha^2\rangle_{\mathrm{PX}} < \langle\alpha^2\rangle_Q$, i.e., the condition assumed here.

We further checked this hypothesis against the other experimental findings that showed differences between the PX and *Q* phases. The higher decay temperature reported for *Q* phase is also consistent with larger tilts. Indeed, departure from 180° of the Fe-CN-Co dihedral angle would decrease the transfer integral. In addition, the disordered character of the tilts would generate a variable range potential that favors

the localization of the Co e_g electrons. In contrast, a mere and isotropic contraction of a regular fcc network would have lowered the decay temperature, according to the results of hydrostatic pressure studies on cobalt hexacyanoferrates[41] and spin-crossover solids.[42] The two-step evolution of the Q phase on heating can also be accounted for assuming first an electronic relaxation, followed by a reduction in the distortions.

At last, the broadening of the magnetic transition and that of the thermal decay reported for the photoexcited phase could originate either from a large distribution of tilt amplitudes despite of a reduced mean value $\langle \alpha^2 \rangle_{PX}$, or else from elastic stresses induced by the growth mode of the photoexcited domains. In that latter case, both the strain and the domain dimensions would influence the ordering (freezing) temperature, whereas the decay temperature will be mainly shifted because of the biaxial stresses between domains. It is also possible that such stresses affect the $[Fe(CN)_6]$ local tilt amplitude and thus widen their distribution.

V. CONCLUSIONS

The present report provides further experimental evidence for complex multistability in photomagnetic Prussian blue derivatives from combined magnetic and synchrotron x-ray powder diffraction experiments. Clear differences in the magnetic properties of the HT quenched phase and of the photoexcited phase were observed, which were not predicted by the two-state Ising-like model used so far to describe the switching properties of these systems. Despite an analogy in their formal electronic configuration, it is necessary to assume a structural deformation that differentiates the two metastable phases. We propose, as "hidden order parameter," the local tilting of the $[Fe(CN)_6]$ polyhedra, which should not be correlated over long distances to retain the $Fm3m$ space group. The larger tilting is observed in the HT phase and in the derived thermally quenched phase. Such tilting weakens the magnetic superexchange interactions and also tend to localize the Co e_g electrons, therefore shifting the decay of the metastable phase to higher temperatures.

The two metastable phases also show different temperature evolution on heating. While the photoexcited phase relaxes back to the ground state, the HT quenched phase shows a two-step conversion, with a first step associated to an electron transfer between Co and Fe and the second step being merely structural. Work is in progress to clarify the structural models for the various intermediate phases from high-resolution synchrotron x-ray powder diffraction measurements. Several questions remain open, such as the static or dynamic nature of the local tilts and their link with intrinsic compositional disorder ($[Fe(CN)_6]$ vacancies, alkali-metal ions or water molecules).

To conclude, most of the Prussian blue analogs are compositionally disordered. The $Fm3m$ symmetry is actually an average over many unit cells of different chemical composition (fractional Na, $[Fe(CN)_6]$ and water contents) and presumably of different degree of deformation (amplitude of the $[Fe(CN)_6]$ local tilt). For most Prussian blue analogs, the ground state is therefore intrinsically disordered. Such a disorder would affect the critical fluctuations for a second-order transition, exemplified here by the ferrimagnetic ordering, as well as the nucleation and growth processes for thermal CTIST and PIPT. This structural disorder seems to be important for a full understanding of the photomagnetic properties but it is much more difficult to study. Short-range correlations could be evidenced through diffuse scattering but good quality single-crystal diffraction data are necessary to analyze such effects (see Ref. 43 for instance).

ACKNOWLEDGMENTS

The authors are indebted to the CNRS (Centre National de la Recherche Scientifique) for financial support and to the ESRF for provision of synchrotron beamtime. They also thank P. Pattison for valuable discussions on the XRD data analyses. E. Codjovi is acknowledged for advices with the photomagnetic measurements and K. Boukheddaden for fruitful discussions. This research activity was supported by the MAGMANET consortium.

*Corresponding author. LPMC, Ecole Polytechnique, 91128 Palaiseau, France. FAX: 00 33 1 69 33 47 99; isabelle.maurin@polytechnique.edu

[1] K. Miyano, T. Tanaka, Y. Tomioka, and Y. Tokura, Phys. Rev. Lett. **78**, 4257 (1997); Y. Okimoto, Y. Ogimoto, M. Matsubara, Y. Tomioka, T. Kageyama, T. Hasegawa, H. Koinuma, M. Kawasaki, and Y. Tokura, Appl. Phys. Lett. **80**, 1031 (2002); M. Fiebig, D. Fröhlich, T. Lottermoser, and R. V. Pisarev, Phys. Rev. B **65**, 224421 (2002).

[2] S. Decurtins, P. Gütlich, C. P. Kohler, H. Spiering, and A. Hauser, Chem. Phys. Lett. **105**, 1 (1984); T. Suzuki, T. Sakamaki, K. Tanimura, S. Koshihara, and Y. Tokura, Phys. Rev. B **60**, 6191 (1999).

[3] O. Sato, T. Iyoda, A. Fujishima, and K. Hashimoto, Science **272**, 704 (1996).

[4] E. Collet, M. H. Lemee-Cailleau, M. Buron-Le Cointe, H. Cailleau, M. Wulff, S. Koshihara, M. Meyer, L. Toupet, P. Rabiller, and S. Techert, Science **300**, 612 (2003).

[5] Y. Moritomo, M. Hanawa, Y. Ohishi, K. Kato, M. Takata, A. Kuriki, E. Nishibori, M. Sakata, S. Ohkoshi, H. Tokoro, and K. Hashimoto, Phys. Rev. B **68**, 144106 (2003).

[6] H. Tokoro, S. Ohkoshi, and K. Hashimoto, Appl. Phys. Lett. **82**, 1245 (2003).

[7] S. Ohkoshi, S. Yorozu, O. Sato, T. Iyoda, A. Fujishima, and K. Hashimoto, Appl. Phys. Lett. **70**, 1040 (1997).

[8] S. Ohkoshi and K. Hashimoto, J. Photochem. Photobiol. C **2**, 71 (2001).

[9] N. Shimamoto, S. Ohkoshi, O. Sato, and K. Hashimoto, Inorg. Chem. **41**, 678 (2002).

[10] A. Goujon, O. Roubeau, F. Varret, A. Dolbecq, A. Bleuzen, and

M. Verdaguer, Eur. Phys. J. B **14**, 115 (2000).
[11] S. Gawali-Salunke, F. Varret, I. Maurin, C. Enachescu, M. Malarova, K. Boukheddaden, E. Codjovi, H. Tokoro, S. Ohkoshi, and K. Hashimoto, J. Phys. Chem. B **109**, 8251 (2005).
[12] M. Nishino, K. Boukheddaden, S. Miyashita, and F. Varret, Phys. Rev. B **72**, 064452 (2005).
[13] J. Wanjflasz and R. Pick, J. Phys. Colloq. **32**, C1–91 (1971); A. Bousseksou, J. Nasser, J. Linares, K. Boukheddaden, and F. Varret, J. Phys. I **2**, 1381 (1992).
[14] P. Huai and K. Nasu, J. Phys. Soc. Jpn. **71**, 1182 (2002); P. Huai and K. Nasu, Phase Transit. **75**, 649 (2002).
[15] T. Tayagaki and K. Tanaka, Phys. Rev. Lett. **86**, 2886 (2001).
[16] N. Huby, L. Guérin, E. Collet, L. Toupet, J. C. Ameline, H. Cailleau, T. Roisnel, T. Tayagaki, and K. Tanaka, Phys. Rev. B **69**, 020101(R) (2004).
[17] H. Oyanagi, T. Tayagaki, and K. Tanaka, J. Lumin. **119**, 361 (2006).
[18] T. Yokoyama, T. Ohta, O. Sato, and K. Hashimoto, Phys. Rev. B **58**, 8257 (1998).
[19] M. Hanawa, Y. Moritomo, A. Kuriki, J. Tateishi, K. Kato, M. Takata, and M. Sakata, J. Phys. Soc. Jpn. **72**, 987 (2003).
[20] M. Hanawa, Y. Moritomo, J. Tateishi, Y. Ohishi, and K. Kato, J. Phys. Soc. Jpn. **73**, 2759 (2004).
[21] T. Yokoyama, M. Kiguchi, T. Ohta, O. Sato, Y. Einaga, and K. Hashimoto, Phys. Rev. B **60**, 9340 (1999).
[22] H. Tokoro, T. Matsuda, S. Miyashita, K. Hashimoto, and S. I. Ohkoshi, J. Phys. Soc. Jpn. **75**, 085004 (2006).
[23] A. Bleuzen, V. Escax, A. Ferrier, F. Villain, M. Verdaguer, P. Münsch, and J. P. Itié, Angew. Chem. Int. Ed. **43**, 3728 (2004).
[24] N. Shimamoto, S. Ohkoshi, O. Sato, and K. Hashimoto, Mol. Cryst. Liq. Cryst. (Phila. Pa.) **344**, 95 (2000).
[25] O. Sato, Y. Einaga, A. Fujishima, and K. Hashimoto, Inorg. Chem. **38**, 4405 (1999).
[26] O. Sato, Y. Einaga, T. Iyoda, A. Fujishima, and K. Hashimoto, J. Phys. Chem. B **101**, 3903 (1997).
[27] H. Romstedt, A. Hauser, and H. Spiering, J. Phys. Chem. Solids **59**, 265 (1998).
[28] A. P. Hammersley, ESRF Internal Report No. ESRF97HA02T, 1997 (unpublished); A. P. Hammersley, S. O. Svensson, M. Hanfland, A. N. Fitch, and D. Häusermann, High Press. Res. **14**, 235 (1996).
[29] G. Champion, V. Escax, C. Cartier dit Moulin, A. Bleuzen, F. Villain, F. Baudelet, E. Dartyge, and M. Verdaguer, J. Am. Chem. Soc. **123**, 12544 (2001) See also V. Gadet, D. M. Bujoli, L. Force, M. Verdaguer, K. E. Malkhi, A. Deroy, J. P. Besses, C. Chappert, P. Veillet, J. P. Renard, and P. Beauvillain, in *Magnetic Molecular Materials*, edited by O. Kahn, D. Gatteschi, J. S. Miller, and F. Palacio (Kluwer, London, 1991) Vol. E198, p. 281 and Refs. 3 and 25.
[30] This temperature dependence of χT presumably arises from a sizeable orbital contribution to the effective magnetic moment, μ. Reports on Co^{II}(HS) and Fe^{III}(LS)-based complexes have shown that μ ranges from 4.2 to $5.3\mu_B$ per ion for the formers [D. H. Martin, in *Magnetism in Solids* (Iliffe, London, 1967) p. 205] and is of the order of $2.4\mu_B$ for $Fe^{III}(CN)_6$ entities [M. F. Tweedle and L. J. Wilson, J. Am. Chem. Soc. **98**, 4824 (1976)] in clear contrast with the spin-only moments, $3.87\mu_B$ and $1.74\mu_B$, respectively. The magnetic-susceptibility data displayed in Fig. 1 for the quasiequilibrium phases are fairly consistent with the upper values of μ reported for these two species.
[31] Several quenching experiments were carried out at 20 or 30 K using various sample amounts and/or sample holders of different heat capacity (see the experimental section). They all gave similar results for the magnetic data characteristic of the HT quenched phase such as the inflection point of the $M_{FC}(T)$ curve at 50 Oe (± 0.2 K), the magnetization value at 5 K under 5 T ($\pm 3\%$), or the decay temperature (less than 1 K difference).
[32] Previous work by Varret *et al.* has evidenced the nonrelaxed character of the magnetic domain structure in the raw photoinduced state, see F. Varret, A. Goujon, and A. Bleuzen, Hyperfine Interact. **134**, 69 (2001).
[33] H. J. Buser, D. Schwarzenbach, W. Petter, and A. Ludi, Inorg. Chem. **16**, 2704 (1977).
[34] O. Masson and A. Ramponi, PEAKOC program, ESRF.
[35] If we assume a phase separation based on chemical heterogeneities, a key point is that the diffraction line splitting occurs at the very first stages, *i.e.* over the first 15–20 K, of the thermally induced spin transition. It is already apparent as a tail at 230 K, temperature at which the conversion fraction can be estimated as less than 9% from the ratio between the integrated intensities of the (220) lines. It implies that the composition gradients, if they exist, are rather small since there is a strong dependency of the CTIST temperatures on the sample composition, roughly 352 K/xNa for the cooling branch in the $Na_xCo[Fe(CN)_6]_y \cdot zH_2O$ series according to Ref. 9. Considering this latter relationship as valid for the sample under study, the sodium content in the two phases would be 0.29 and 0.35, that is to say roughly comparable to the uncertainty of the elemental analysis. The split diffraction lines cannot arise from such a slight variation in the Na or $[Fe(CN)_6]$ vacancy content because similar results (main cubic phase and secondary phase of lower symmetry, almost in the same proportion as in the sample investigated here) were also encountered for another sample of nominal composition $Na_{0.45}Co[Fe(CN)_6]_{0.78} \cdot 3.3H_2O$.
[36] S. Pillet, V. Legrand, M. Souhassou, and C. Lecomte, Phys. Rev. B **74**, 140101(R) (2006).
[37] S. V. Grigoriev, S. A. Klimko, W. H. Kraan, S. V. Maleyev, A. I. Okorokov, M. T. Rekveldt, and V. V. Runov, Phys. Rev. B **64**, 094426 (2001).
[38] M. Campostrini, A. Pelissetto, P. Rossi, and E. Vicari, Phys. Rev. E **60**, 3526 (1999).
[39] S. Margadonna, A. N. Fitch, and K. Prassides, J. Am. Chem. Soc. **126**, 15390 (2004).
[40] K. W. Chapman, P. J. Chupas, and C. J. Kepert, J. Am. Chem. Soc. **128**, 7009 (2006).
[41] I. Maurin, E. Codjovi, K. Boukheddaden, and F. Varret (unpublished).
[42] J. Jeftic, H. Romstedt, and A. Hauser, J. Phys. Chem. Solids **57**, 1743 (1996); J. Jeftic and A. Hauser, Chem. Phys. Lett. **248**, 458 (1996), and references therein.
[43] P. Franz, C. Ambrus, A. Hauser, D. Chernyshov, M. Hostettler, J. Hauser, L. Keller, K. Krämer, H. Stoeckli-Evans, P. Pattison, H.-B. Bürgi, and S. Decurtins, J. Am. Chem. Soc. **126**, 16472 (2004).